Biosensors and Bioelectronics 208 (2022) 114236

Contents lists available at ScienceDirect

Biosensors and Bioelectronics

journal homepage: www.elsevier.com/locate/bios

# Highly sensitive and reliable detection of microRNA for clinically disease surveillance using SERS biosensor integrated with catalytic hairpin assembly amplification technology

Shuyun Weng [a,1], Duo Lin [a,1], Shuxia Lai [a], Hong Tao [a], Tong Chen [a], Min Peng [a], Sufang Qiu [b], Shangyuan Feng [a,*]

[a] Key Laboratory of OptoElectronic Science and Technology for Medicine, Ministry of Education, Fujian Provincial Key Laboratory for Photonics Technology, Fujian Normal University, Fuzhou, 350007, China
[b] Fujian Cancer Hospital & College of Clinical Medicine for Oncology, Fujian Medical University, Fuzhou, 350001, China

ARTICLE INFO

*Keywords:*
Surface-enhanced Raman scattering (SERS)
Catalytic hairpin assembly (CHA)
MicroRNAs
Breast cancer
Diagnosis and prognosis

ABSTRACT

MicroRNAs (miRNAs) play an important regulatory role in several diseases, especially as a class of promising biomarkers for cancer diagnosis and prognosis. Here, a biosensor based on surface enhanced Raman spectroscopy (SERS) combined with catalytic hairpin assembly (CHA) amplification technology was developed for ultrasensitive detection of miRNA-21 and miRNA-155 in breast cancer serum. By using CHA strategy, the extremely low concentration of target microRNA in human serum can be significantly amplified through the re-hybridization with thousands of hairpin probes to trigger amplification cycles. Besides, a sandwich SERS sensing chip with numerous hot spots and signal self-calibration was built through the linkage between two-dimensional Au–Si substrate and upper Ag@4-MBA@Au core-shell nanoparticles. Using this specially-designed biosensing platform, a low detection limit of 0.398 fM and 0.215 fM with a dynamic range from 1 fM to 10 nM can be achieved for the detection of miRNA-21 and miRNA-155, respectively. Additionally, the analysis of these two miRNAs in serum samples is capable of identifying the breast cancer subjects from normal ones with 100% of accuracy, as well as potentially evaluating the molecular types and prognosis for breast cancer. These results demonstrate that the proposed SERS with CHA technology would be an alternative method for highly sensitive and reliable detection of miRNA biomarkers contributing to breast cancer diagnosis and prognosis.

## 1. Introduction

Breast cancer is the most commonly diagnosed cancer among women, with 226,419 new cases and 684,996 deaths worldwide in 2020 (Chowdhury et al., 2021; Sung et al., 2021). Previous studies have confirmed that some microRNAs (miRNAs) are involved in the development and progression of cancer (Zhu et al., 2020). The miRNAs are non-coding RNAs with 21–25 nucleotides that exert gene regulation by binding to target genes and inhibiting translation (Chen et al., 2019b; Qin et al., 2021). They will affect various aspects of breast cancer development and progression, such as cell proliferation, migration, invasion, and differentiation, by regulating signaling pathways (Abolghasemi et al., 2020). Iorioet al. firstly reported the association of miRNAs with breast cancer in 2005. Results showed that miRNA-21 and miRNA-155 were upregulated in breast cancer, while miR-10b, miR-125b and miR-145 were downregulated (Iorio et al., 2005). Following that, a growing number of studies further demonstrated that microRNAs are potentially biomarkers for breast cancer diagnosis and prognosis (Kandettu et al., 2020). However, traditional miRNA detection techniques which include Northern blotting (De la Rosa and Reyes, 2019; Zia and Flynt, 2018), quantitative real-time polymerase chain reaction (qRT-PCR) (Damanti et al., 2021; Hu et al., 2021), fluorescence (Guk et al., 2019; Ye et al., 2017) and electrochemisty (Chen et al., 2017) have the disadvantages of requiring expensive and complex instrumentation, complicated operation steps, time consuming and low sensitivity [9]. Moreover, because of the low abundance of miRNAs in cancer and the high sequence homology, accuracy detection remains challenging [8]. According to statistics, patients with early-stage breast

* Corresponding author.
*E-mail address:* syfeng@fjnu.edu.cn (S. Feng).
[1] Shuyun Weng and Duo Lin are co-first authors.

https://doi.org/10.1016/j.bios.2022.114236
Received 30 January 2022; Received in revised form 22 March 2022; Accepted 29 March 2022
Available online 1 April 2022

cancer have a survival rate of 98% with treatment, while the survival rate of patients with advanced breast cancer decreases to 27% (Song and Giovannucci, 2016). As a result, there is an urgent need for a convenient, rapid, sensitive and reliable method for early diagnosis and prognosis prediction of breast cancer.

Recently, surface-enhanced Raman scattering (SERS), a nano-photonic technology has been widely used for ultrasensitive detection of cancer due to its high sensitivity, specific fingerprint, fast acquisition, photobleaching resistance and multiplexed detection ability (Driscoll et al., 2013; Ma et al., 2018). Sensitive detection of cancer-related nucleic acid is one of the most important applications of SERS for cancer diagnosis and prognosis, in which two kinds of sensing mechanisms are commonly used. One category consists of non-specific detection based on label-free SERS by mixing the metal nanoparticles with nucleic acid. Although convenient and capable of obtaining the intrinsic spectral signals of nucleic acid, this assay suffers from low specificity, being susceptible to environmental interferences and low multiplexed ability. The other one is using Raman reporter to specifically bind to the target nucleic acid to achieve specific quantitative detection (Garcia-Rico et al., 2018). For example, Jiamin Wu et al. proposed a magnetic-assisted sandwich SERS biosensor for multiplex detection of three hepatocellular carcinoma-related miRNAs(Wu et al., 2021a). Jing Su et al. reported a DNA-mediated gold and silver nanomushroom with internal nanogaps for simultaneous SERS detection of multiple DNAs and RNAs(Su et al., 2017). Although promising, some issues associated with label SERS for nucleic acid detection remains to be addressed such as the impacts from laser fluctuations and environmental changes during the measurement process. Besides, miRNAs are extremely short sequences that exhibit a high degree of homology (Roush and Slack, 2008) and have a markedly low concentration with only 0.01% of the total RNA mass in the pM range in plasma (Dong et al., 2013; Mitchell et al., 2008; Williams et al., 2013). This requires assays that are sufficiently sensitive and also show a dynamic range spanning at least four orders of magnitude (Williams et al., 2013). Catalytic hairpin apparatus (CHA) is an isothermal amplification technique based on a cascade DNA reaction that produces 100-fold catalytic amplification and becomes a widely used technique for amplifying biosensors (Zhuang et al., 2014). Compared with enzyme-assisted amplification methods such as rolling circle amplification (RCA), strand displacement amplification (SDA) and loop-mediated isothermal amplification (LAMP), CHA has the advantage of low cost, easy storage and simple reaction conditions (Zhang et al. 2017, 2018b). In contrast to other enzyme-free amplification methods, including hybridization chain reaction (HCR), DNAzyme and entropy driven circuits (EDC), CHA offers the advantages of higher catalytic efficiency, lower background signal and simpler stability (Zhou et al., 2018). Therefore, label SERS-based miRNA detection needs to be further explored and improved for the future clinically practical application.

In this study, a novel biosensor combining SERS with CHA amplification technology for ultra-sensitive detection of miRNA-21 and miRNA-155. The isothermal amplification technique based on catalytic hairpin assembly (CHA) with the advantages of low background signal and high turnover rate (Chen et al., 2019a; Si et al., 2020; Wang et al., 2021) was used to amplify the ultra-low concentration of target miRNA. Then, a sandwich SERS biosensing model with signal self-calibration function was built to dramatically increase the Raman signals of SERS reporters and decrease the interferences from surrounding environment. Finally, the feasibility of this SERS-based biosensor was evaluated for the diagnosis and prognosis prediction of breast cancer.

## 2. Experimental section

### 2.1. Materials

All qualified DNA oligonucleotides, miRNA, Diethyl pyrocarbonate (DEPC)− water, 1x TE buffer and RNase inhibitor were purchased from Sangon Biological Engineering Technology & Services Co., Ltd (Shanghai, China). The detailed sequences of nucleic acids used in this study are listed in Table S1. Then all solutions were treated with 0.1% DEPC followed by autoclaving. The 50bp DNA Ladder and agarose was purchased from Beijing Solarbio Science & Technology Co., Ltd (Beijing, China). Hydrogen tetrachloroaurate hydrate ($HAuCl_4{\cdot}4H_2O$), silver nitrate ($AgNO_3$), dichloromethane ($CH_2Cl_2$), anhydrous ethanol ($CH_3CH_2OH$), n-hexane ($C_6H_{14}$) and trisodium citrate dihydrate (TCD, $Na_3C_6H_5O_7{-}2H_2O$) were purchased from Sinopharm Chemical Reagents Co., Ltd (Shanghai, China). The 4-mercaptobenzoic acid (4-MBA) and polyvinylpyrrolidone (PVP) were bought from Shanghai Macklin Biochemical Co., Ltd (Shanghai, China). Ascorbic acid (AA) was obtained from Sigma−Aldrich Co., Ltd. (Shanghai, China). 6-Mercapto-1-hexanol (MCH) was purchased from J&K Scientific Co., Ltd (Beijing, China). Ultrapure (Up) water (resistivity of 18.2 MΩ cm) was used throughout the process, produced by the Milli-Q gradient system. All glassware was soaked in chromic acid for 24 h, rinsed at least five times with Up water and dried in an oven. The all solution was subsequently treated with 0.1% DEPC and then autoclaved.

### 2.2. Instruments

The UV–visible spectra were obtained with a Lambda 950 (PerkinElmer, USA). Dynamic light scattering (DLS) and zeta potential measurements were performed by a Malvern Zetasizer NanoZ (Malvern Panalytical, UK). The transmission electron microscopy (TEM) images were obtained with FEI Talos F200s (FEI, USA). The scanning electron microscope (SEM) images were obtained with a Zeiss Sigma 300 (Zeiss, Germany). High-resolution SERS spectra were recorded with a HORIBA Details XploRA™PLUS (HORIBA, Japan) with a 785 nm laser source. The Raman spectrometer was calibrated prior to the measurements using a standard Raman spectrum in silicon with a first-order Raman peak centered at 520 $cm^{-1}$.

### 2.3. Synthesis of AuNPs, AgNPs and Au@4-MBA@Ag NPs

Au NPs were prepared by the trisodium citrate dihydrate reduction method according to Grabar's report (Wu et al., 2021b). 1 ml of 1% $HAuCl_4$ was added to 99 ml Up water and stirred vigorously until boiling. Then, 1 ml of 1% TCD was added rapidly, making the color of the solution from light yellow to dark red. Subsequently, the reaction was kept stirring and boiling for 20 min to ensure complete reaction. After that, the solution was cooled down to room temperature and stored at 4 °C.

Ag NPs were prepared using the sodium citrate reduction method reported by Lee et al. (Madzharova et al., 2020). 17 mg $AgNO_3$ were added to 100 ml Up water and stirred vigorously until boiling. 3 ml of 1% TCD was added and continued to stir vigorously for 1 h to make the solution gradually change its color from clear to gray-green. 2 ml of Ag NPs solution was centrifuged and the supernatant was discarded and re-suspended. Then add 10 μl of 1 mM 4-MBA and stir it for 12 h to obtain Ag@4-MBA NPs solution. Add 2.5 ml of 200 mM NaOH, 2.5 ml of 100 mM AA and 50 μl Ag@4-MBA NPs to 10 ml of 1 mM PVP solution and stir the mixture for 10 min. Then add 0.1 mM chloroauric acid dropwise at 100 μl/min and continue to react for 30 min. The solution was centrifuged at 7000 rpm for 8 min and re-suspended in Up water for three times. Finally, the washed solution was stored at 4 °C.

### 2.4. Synthesis of Au–Si chip

Silicon chips with Au NPs on the surface were synthesized using Lin's method (Lin et al., 2020). First, 2 ml Au NPs were centrifuged and re-suspended in 1 ml 1% PVP followed by centrifugation and washing. The precipitate was re-suspended in anhydrous ethanol to obtain Au@PVP NPs. 4 mm × 4 mm Si Chip were placed in anhydrous ethanol solution for 10 min and dried for use. Mix 100 μl of Au@PVP NPs with 1

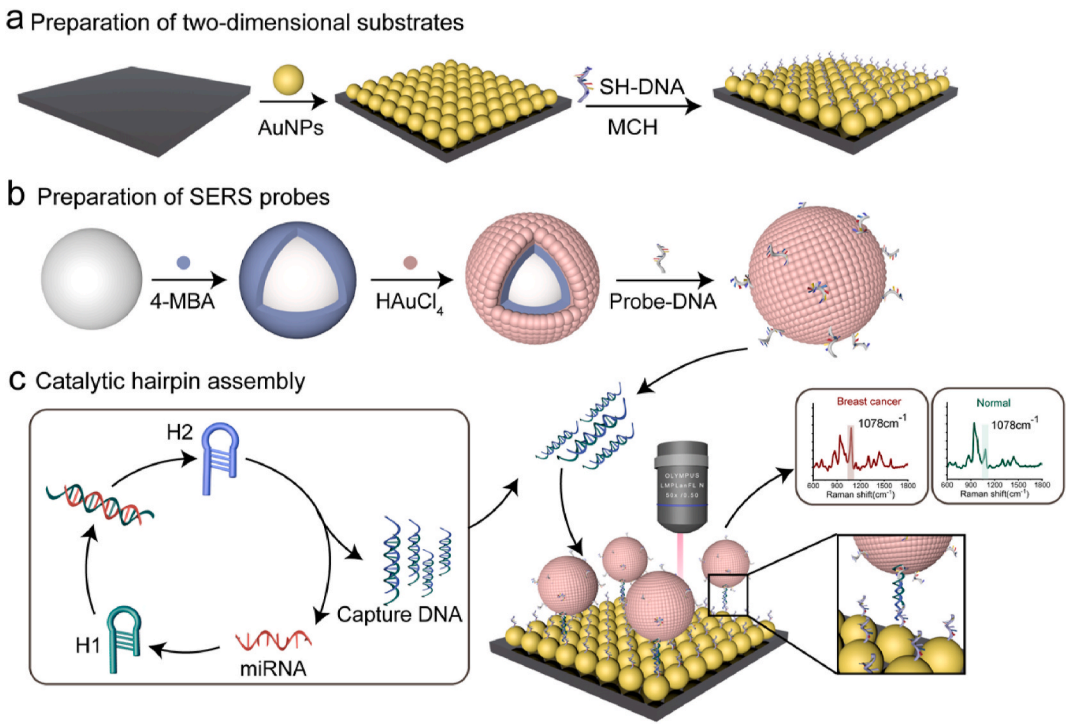


**Scheme 1.** Schematic illustrations of (a) the preparation of a two-dimensional substrate Au@DNA-Si chip, (b) the preparation of SERS probes (Ag@4-MBA@Au@DNA NPs) and (c) the principle of the SERS biosensor coupled with CHA for the detection of miRNA.

ml of $CH_2Cl_2$ and 2 ml of Up water for 30 s. Then add 200 μl of $C_6H_{14}$ until the upper layer was separated before removing the liquid. The silicon chips were tilted and immersed in the liquid to form a gold film with Au NPs on the wafer surface. The chips were dried at room temperature before use.

### 2.5. Assembly of SERS sensors

All sulfhydryl-modified DNAs were first activated with equal concentrations of TCEP for 1 h.

Preparation of Au@4-MBA@Ag@DNA NPs: Take the activated probe-DNA and mix the solution thoroughly with 100 μl Ag@4-MBA@Au NPs solution. The solution was then incubated for 30 min at room temperature and frozen at - 20 °C for 2 h. The solution was then thawed at room temperature to obtain Au@4-MBA@Ag@DNA NPs. The solution was washed by centrifugation and re-suspended in 100 μl of Up water.

Preparation of Au@DNA-Si Chip: 100-fold diluted SH-DNA solution was dropped onto Au–Si Chi and incubated overnight at room temperature for 12 h, followed by 3 times of washing with Up water. The Au@DNA-Si Chip were soaked with 100 μl of 40 μM MCH for 30 min to seal the surface. Then, the chips were washed 3 times and left to dry at room temperature.

### 2.6. Collection of clinical blood samples

The blood serum samples from 30 healthy human subjects and 30 breast cancer patients were collected from Fujian Cancer Hospital, and the miRNA concentrations in the serum were measured using SYBR Green qPCR Master Mix kits (ABI QuantStudio 5 Q5, USA). 1 ml of blood was collected from each study subject between 7:00 and 8:00 a.m. after 12 h of overnight fasting. Each sample was centrifuged at 1000 rpm for 10 min to isolate the serum, and the supernatant was collected and stored at −80 °C for use. Informed consent was obtained from all participants. The patient characteristics are shown in Table S3.

### 2.7. miRNA extraction and detection

The 100 μM miRNA was diluted with DEPC solution to 10 nM, 1 nM, 100 pM, 10 pM, 1 pM, 100 fM, 10 fM and 1 fM, respectively. 10 μl of miRNA-21 at different concentrations were added to 100 μl of Au@SH-DNA@ROX-DNA NPs solution and the reaction was carried out at room temperature for 2 h. After centrifugation, the precipitate was dropped onto an aluminum plate and dried slowly at room temperature before SERS measurement.

10 μl of 1 μM H1 and 10 μl of different miRNA concentrations were mixed thoroughly and 10 μl of 1 μM H2 was added for 2 h at room temperature to obtain Capture DNA double-stranded solution. 100 μl Au@4-MBA@Ag@DNA NPs and Capture DNA were mixed thoroughly and dropped onto Au@DNA-Si Chip and incubated together at room temperature for 2 h. The chips were washed with PBS buffer and then washed with Up water and dried at room temperature for the SERS assay.

### 2.8. Agarose gel electrophoresis

Hairpin DNA was formed by annealing at 95 °C for 10 min and then cooling to room temperature. 10 μM miRNA was added to 1 μm H1 and 1 μM H2, and then incubated at 37 °C for 2h. CHA results were analyzed by agarose gel electrophoresis (2.5%, w/w) at 130 V in 1 × TAE buffer for 40 min.

### 2.9. SERS measurement

After wavelength calibration of the Raman spectrometer with a single crystal silicon 520 $cm^{-1}$ Raman peak, the Raman spectral signal was collected in the range of 600–1800 $cm^{-1}$ using an excitation wavelength of 785 (laser power of 5.8 mW) with an integration time of 5s and 50 × objective.

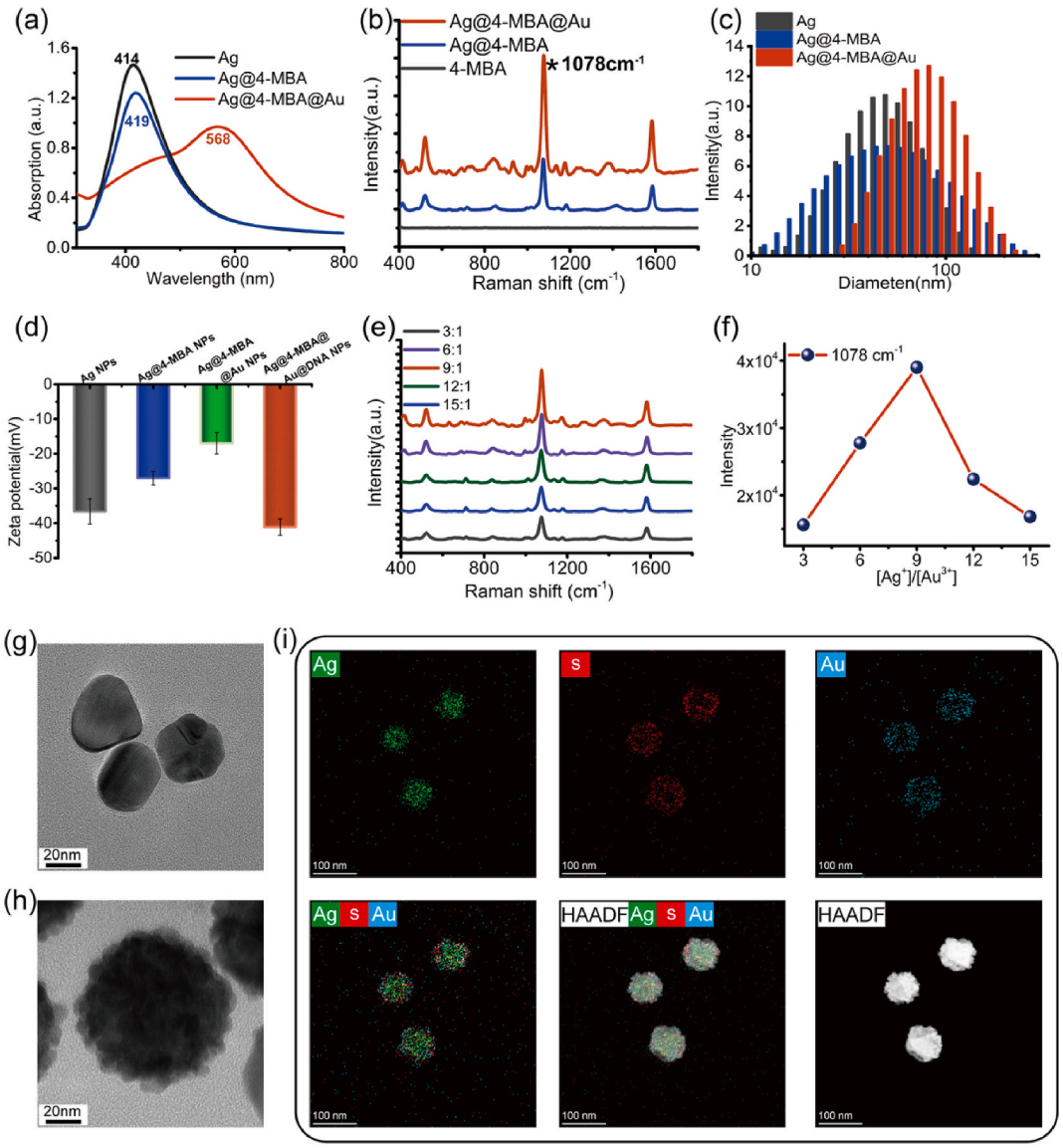


**Fig. 1.** Characterization of SERS probe (Ag@4-MBA@Au@DNA NPs). (a–d) UV–Vis spectra, SERS spectra, size distribution and Zeta potentials of the Ag NPs, Ag@4-MBA NPs and Ag@4-MBA@Au NPs. (e) Raman signals and (f) the intensity of single Raman peak at 1078 $cm^{-1}$ corresponding to Ag@4-MBA@Au NPs with different shell thicknesses. TEM image of (g) Ag NPs and (h) Ag@4-MBA@Au NPs. (i) EDS elemental mapping of independent Ag (green), S (red) and Au (blue), as well as merged image of Ag@4-MBA@Au NPs.

## 3. Results and discussion

### *3.1. Fabrication of miRNA sensing platform based on SERS combined with CHA amplification technology and sensing mechanism*

The principle of the SERS-based miRNA biosensor is illustrated in Scheme 1. The scheme consists of three parts: (I) A two dimensional SERS substrate was prepared by loading Au NPs on the Si chip via a three-phase self-assembly method. Then, the SH-DNA was modified on the Au–Si chip to Capture DNA products, in which the MCH was finally used to seal the metal surface to minimize the non-specific adsorption of single-stranded DNA (Scheme 1a). (II) A layer-by-layer modification approach was used to prepare the SERS probes. First, we modified the surface of Ag NPs with 4-MBA as the Raman report molecule. Then, the outer Au layer were generated by the reduction process on the Ag@4-MBA surface and attached to the surface to finally form core-shell NPs (Ag@4-MBA@Au NPs). Probe-DNA was finally ligated to the surface of Ag@4-MBA@Au NPs by the freezing method (Scheme 1b). The second order peak of Si 936 $cm^{-1}$ was used as an internal standard calibration and the Raman signal molecule located in the middle layer of the silver core and gold shell, thus ensuring that the nature, spatial structure and quantity of the Raman signal molecule 4-MBA were not influenced by the detection environment and guaranteeing the reliability of the assay results. (III) The CHA cycle amplification system can specifically recognizes the miRNA and then generates Capture DNA. Specifically, the number of base complementary pairing bases of miRNA with H1 was more than that in the complementary stem-loop portion of H1 on its own, allowing the hairpin structure of H1 to be opened to form a miRNA-H1double strand. As H2 had more base complementary pairings with H1, H2 displaced the miRNA by competitive binding to form Capture DNA while the released target miRNA induced the next cycle. In turn, H1–H2 formed a stable double strand for trapping the SERS probe to the Au@DNA-Si chip (Scheme 1c).

In the presence of target miRNA, the CHA cycling system will be stimulated to produce a large amount of the Capture DNA, the ends of which bind to probe-DNA on the SERS probe and SH-DNA on the two-dimensional Au@DNA-Si substrate, respectively. Consequently, a sandwich SERS sensing chip with a large number of “hot spots” and the

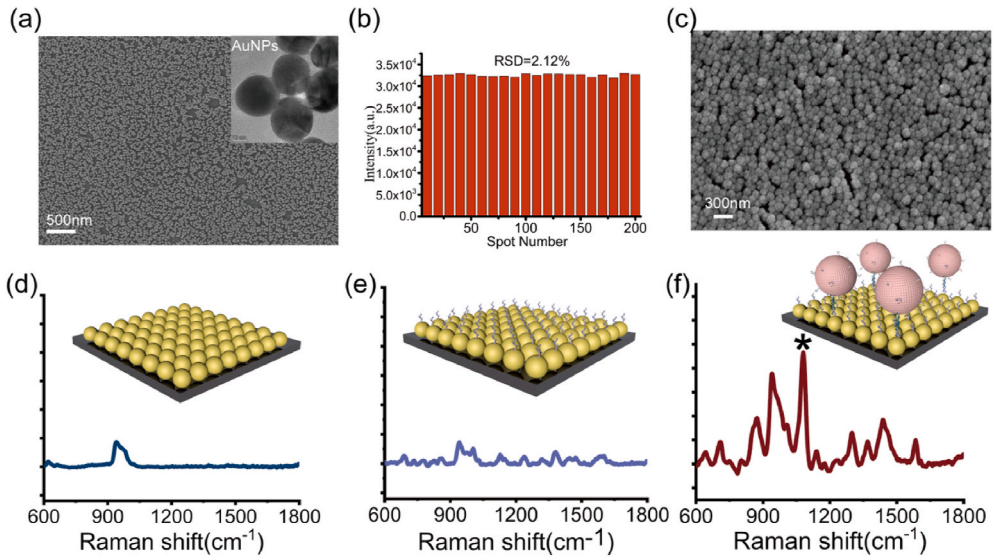


**Fig. 2.** Preparation and characterization of 2D substrate. (a) SEM image of Au–Si chip. Inset: TEM image of Au NPs. (b) Raman signals at 1078 $cm^{-1}$ from different positions of the Au–Si chip. (c) SEM image of sandwich biosensor (Au@4-MBA@Au@DNA NPs-Au@DNA-Si chip). SERS spectra of (d) Au-si chips, (e) Au@DNA-si chips and (f) sandwich nanostructure SERS biosensor.

signal self-calibration function were constructed.

### 3.2. Characterization of the SERS biosensor

Fig. 1a showed there was a UV–Vis absorption peak at 414 nm for bare Ag NPs, and this peak was shifted to 419 nm after modifying the surface of Ag NPs with Raman reporter molecules (4-MBA) by gold-sulphur bonding. After that, the outer gold layer was successfully grown to form core-shell structure (Ag@4-MBA@Au) with the evidence that two broad absorption peaks located at 430 nm and 520 nm were generated (Fig. 1a) as well as the size of nanoparticle increased from 40 ± 5 nm (Ag NPs) to 85 ± 5 nm (Ag@4-MBA@Au) according to dynamic light scattering analysis (Fig. 1c). The morphology of Ag NPs and Ag@4-MBA@Au was further studied by TEM as shown in Fig. 1g and h, respectively. Notably, the surface morphology of the core-shell NPs was relatively unusual where the Au shell was generated through lots of small gold NPs on the surface of the silver core. This would increase the roughness of the core-shell NPs surface, help generating a large number of "hot spots" and consequently enhancing the SERS signal. To better visualize the structure of these core-shell NPs, the STEM element mapping analysis (Fig. 1i) was performed to show the spatial distribution of elements Ag (from the silver core only, green), S (from the embedded 4-MBA molecule only, red), Au (from the gold shell only, blue) and merged image of them, demonstrating that the SERS reporter 4-MBA was well embedded between Ag core and Au layer to form Ag@4-MBA@Au NPs. More importantly, the Raman signals of 4-MBA can be significantly enhanced via the core-shell nanostructure by comparing Raman signals at 1078 $cm^{-1}$ between 4-MBA and Ag@4-MBA@Au (Fig. 1b). Additionally, the enhanced effect for 4-MBA was evaluated by adjusting the ratio of $[Ag^{+}]/[Au^{3+}]$ to generate different thickness of the outer Au layer. At the same time, with the gradual increase of the thickness the absorption peaks are approaching toward 600 nm, implying that the properties of Ag NPs are weakening (Fig. S1), which fits well with the conventional Mie scattering theory and the support of the dielectric data (Bruzzone et al., 2003). Fig. 1e and f shows the strongest Raman signal for 4-MBA can be achieved when the $[Ag^{+}]/[Au^{3+}]$ ratio was set to 9:1. As the thickness of the gold shell becomes larger, the laser excitation of the 4-MBA molecule becomes weaker due to the damping effect of the shell, and the thicker shell also hinders the output of the Raman signal from the 4-MBA. In addition, the greater thickness of the shell may affect its electromagnetic field coupling to the silver core, reducing the electromagnetic enhancement (Zhang et al., 2018a). It is worth noting that embedding the Raman reporter molecule between the metal core and shell layer not only provides a strong signal, but also reduces the interference from surrounding environment, contributing to the subsequent accurate and reliable quantitative detection (Kleinman et al., 2013; van der Hoeven et al., 2021). The change of surface charge at each stage of the assembly process of Ag@4-MBA@Au NPs was also detected by zeta potential. As shown in Fig. 1d, after wrapping 4-MBA onto Ag NPs, the zeta potential increased from −36.63 mV to −27.02 mV which confirmed the successful wrapping of 4-MBA onto the Ag nucleus surface. With the reduction of Au to the Ag@4-MBA surface, the zeta potential went up to −16.94 mV to form the core-shell nanostructure. Then, we fast linked probe-DNA to Ag@4-MBA@Au NPs surface by freezing method, in which the potential dropped to −41.11 mV due to the negative charge of DNA.

Next, the two-dimensional SERS substrate was prepared by loading the AuNPs onto Si chips using oil-water separation method. Fig. 2a showed that a uniform monolayer of Au NPs above the Si chip can be obtained. In order to further assess feasibility of this prepared 2D substrate for SERS assay, we randomly measured 200 spots on this substrate and compared the signal variation from the characteristic Raman peak at 1078 $cm^{-1}$ after incubation with standard substance. Results showed that the relative standard deviation (RSD) of Raman signals from different positions was only 2.12% using this Au–Si chip, indicating the excellent homogeneity of this 2D SERS substrate (Fig. 2b). After that, the Ag@4-MBA@Au@DNA NPs were attached to the surface of the Au@DNA-Si chip via Capture DNA to form the sandwich nanostructure as the SERS biosensor, which can be clearly seen from SEM image in Fig. 2c.

Meanwhile, we characterized the Raman features from Au@Si chip to final sandwich nanostructure-based biosensor (Au@DNA-Si attached with Ag@4-MBA@Au@DNA NPs). Fig. 2d showed a clear Raman peak at 936 $cm^{-1}$ from Si when measuring the Au–Si substrate. After modifying the DNA linker on the surface of Au–Si substrate, more Raman signals from nucleic acid bases existed (Fig. 2e). In the presence of Capture DNA, the sharp Raman peak from 4-MBA at 1078 $cm^{-1}$ appeared (Fig. 2f), which further confirmed the successful construction of sandwich nanostructure-based SERS sensing model for target miRNA detection.

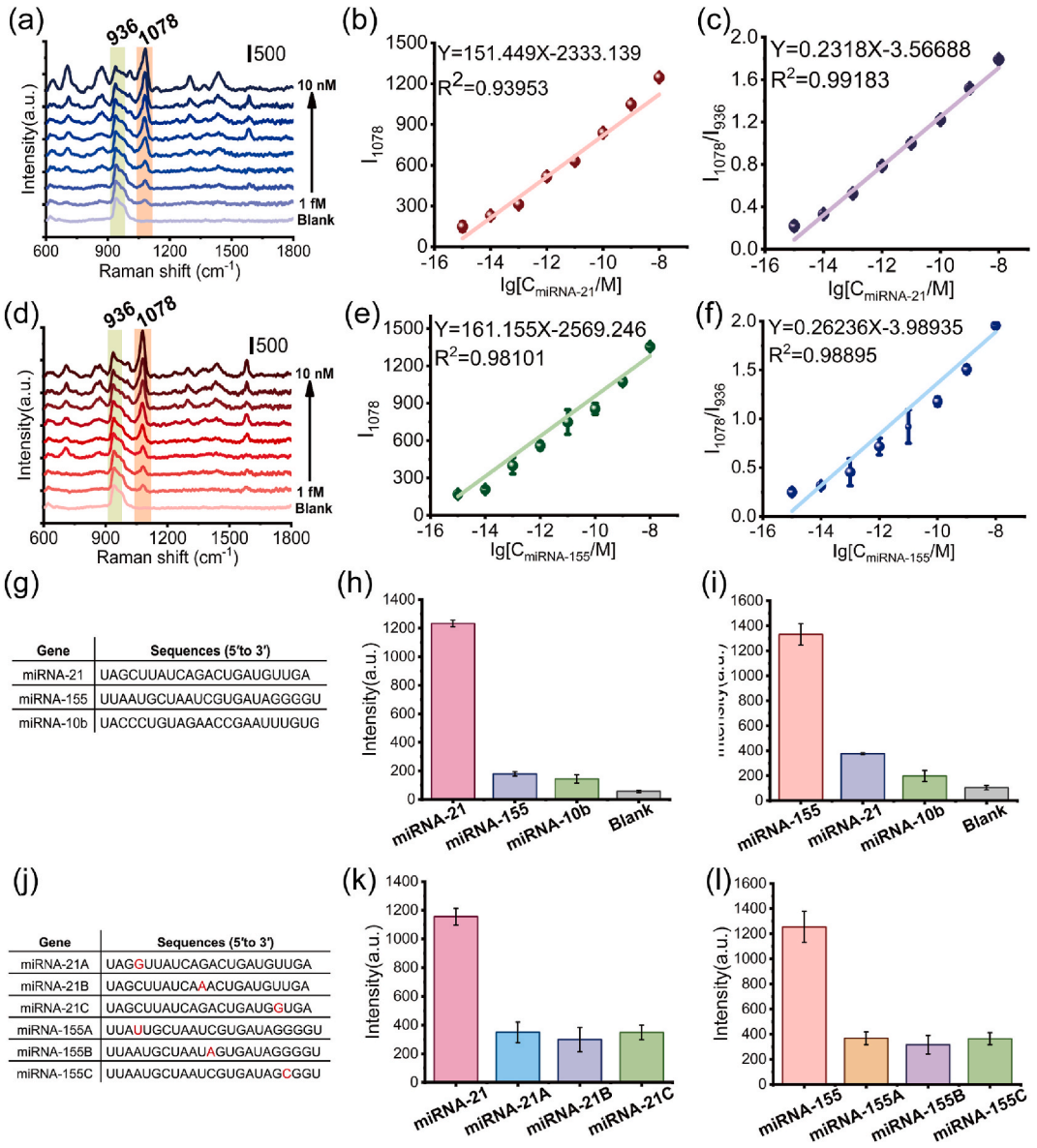


| Gene | Sequences (5′to 3′) |
|---|---|
| miRNA-21 | UAGCUUAUCAGACUGAUGUUGA |
| miRNA-155 | UUAAUGCUAAUCGUGAUAGGGGU |
| miRNA-10b | UACCCUGUAGAACCGAAUUUGUG |

| Gene | Sequences (5′to 3′) |
|---|---|
| miRNA-21A | UAGGUUAUCAGACUGAUGUUGA |
| miRNA-21B | UAGCUUAUCAAACUGAUGUUGA |
| miRNA-21C | UAGCUUAUCAGACUGAUGGUGA |
| miRNA-155A | UUAUUGCUAAUCGUGAUAGGGGU |
| miRNA-155B | UUAAUGCUAAUAGUGAUAGGGGU |
| miRNA-155C | UUAAUGCUAAUCGUGAUAGCGGU |

**Fig. 3.** Ultra-sensitive, and reliable SERS biosensor for miRNA detection. SERS spectra of sensing chip with different concentrations of (a) miRNA-21 and (d) miRNA-155. linear relationship of (b) miRNA-21 and (e) miRNA-155 concentrations on SERS intensity ($I_{1078}$). Linear relationship for SERS intensity ($I_{1078}/I_{936}$) as a function of (c) miRNA-21 and (f) miRNA-155 concentration. (g)Sequence list of miRNA-21, miRNA-155 and miRNA-10b. Selectivity of the detection of (h) miRNA-21 and (i) miRNA-155, with the interfering substances presented at the same concentration. (j) Sequence list of the 3 single base mutations (A–C: 5′ end, midpoint and 3′ end) of miRNA-21 and miRNA-155. (k) Single base mutation selectivity for (k) miRNA-21 and (l) miRNA-155 with interfering substances presented at the same concentrations.

### 3.3. Ultra-sensitive SERS biosensor for miRNA detection

The above-mentioned SERS biosensor integrated with RNA recycling amplification system via CHA was then used for miRNAs detection. First, we used agarose gel electrophoresis to verify that the CHA process occurs according to our design (Fig. S2). It can be found that in the absence of miR-155, H1 and H2 remained stable (lane 5). After the addition of miR-155, a new band appeared and moved slower than H1 and H2. This indicated that H1 and H2 were consumed to form the expected product (Scheme 1c). The double-stranded DNA produced by CHA next acted as a key linker, anchoring the above SERS reporter to the bottom SERS chip in this sensing model. Therefore, the signal (1078 $cm^{-1}$) from SERS reporter can be only observed when presence of target miRNA. Besides, the intensity of the reporter was directly proportional to the concentration of the DNA products that were determined by target miRNA. Here, two miRNA standard samples (miRNA-21 and miRNA-155) with different concentration were used to test the proposed SERS biosensor (Fig. 3). In both assays for miRNA-21 and miRNA-155, the peak intensity of the Raman reporter (4-MBA) at 1078 $cm^{-1}$ gradually increased as the concentration of target miRNA increases from 1 fM to 10 nM. Meanwhile, the Raman signals from Au–Si chip at 936 $cm^{-1}$ maintained relatively stable, indicating this peak was not susceptible to the change in target miRNA and could be an ideal internal standard signal.

Fig. 3a and d indicated that the spectral signal of SERS reporter (4-MBA) at 1078 $cm^{-1}$ gradually elevated as the concentration of two miRNAs increased from 1 fM to 10 nM, respectively. We next performed the linearization analysis using the absolute peak intensity of Raman reporter at 1078 $cm^{-1}$ against the different concentrations of miRNA-21 (Fig. 3b) and miRNA-155 (Fig. 3e), respectively. The limit of detection (LOD) of 0.407 fM and 0.944 fM with linear regression values ($R^2$) of 0.93953 and 0.98101 for miRNA-21 and miRNA-155, respectively, can be achieved at a broad linear range from 1 fM to 10 nM. When applying

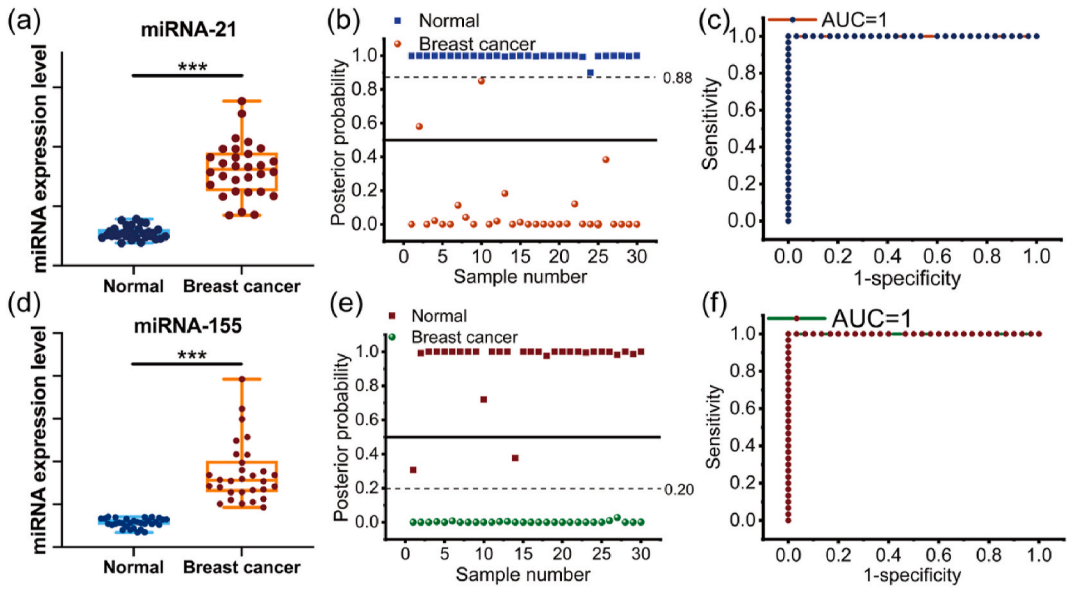


**Fig. 4.** SERS biosensor for miRNA analysis of blood samples from breast cancer patients. Box plots show the difference in the expression levels of (a) miRNA-21 and (d) miRNA-155 in breast cancer (n = 30) and healthy humans (n = 30). Posterior probability scatter plot comparing breast cancer patients and healthy individuals based on (b) miRNA-21 and (e) miRNA-155 SERS data. Receiver operating characteristic (ROC) curves of classification results for breast cancer generated from PCA-LDA analysis based on (c)miRNA-21 and (f) miRNA-155. ***P value < 0.001.

the signals from internal standard (936 $cm^{-1}$) to calibrate that of SERS reporter, the $R^2$ value can be further improved to 0.99183 and 0.98895 for miRNA-21 and miRNA-155 (Fig. 3c and f), indicating the better linear relationship between ratio value ($I_{1078}/I_{936}$) and the concentration of target miRNA. In addition, the LOD was also optimized to 0.398 fM for miRNA-21 and 0.215 fM for miRNA-155, after the calibration process of internal standard. This may be attributed to the fact that the probe signal of this biosensor might vary under the fluctuations of laser power and changes in the surrounding environment during the SERS measurement. Notably, the intensity variations from these external factors simultaneously happened to the internal standard. Therefore, using internal standard to calibrate the absolute signals of SERS reporter is a reasonable and ideal solution to avoid potential and uncontrollable interferences.

Meanwhile, the standard curves of miRNA-21 and miRNA-155 were detected by qRT-PCR absolute quantification method. Results showed that the LODs of miRNA-21 and miRNA-155 were 2.28 fM and 0.45 fM (Table S2, Fig. S3), which is inferior to that detected by the proposed SERS biosensor. Besides, SERS has the advantages of low cost, low instrument dependence and simple operation. To further validate the specificity of this sensor, we performed interference experiments using other miRNAs with the fact that the sensor only has obvious signal output in the presence of the target miRNA (Fig. 3g–i). Furthermore, a series of miRNA sequences with single point mutations at the 5′, 3′-end and mid points of the miRNA-155 and miRNA-21 sequence was designed to evaluate the ability of the biosensor for distinguishing the miRNAs with high homology. It was also showed that only target miRNA exhibited significantly strong SERS signal (Fig. 3j–l). These results suggest that the high specificity of our designed SERS sensor allows accurate detection of miRNAs at the molecular level, without interference from other substances (Lee et al., 2019; Song et al., 2022). In addition, we compared the performance of the SERS biosensor developed in this study with existing miRNA and nucleic acid detection methods listed in Table S2(Chang et al., 2019; Gong et al., 2021; Xu et al., 2014). Our miRNA biosensor was found to be superior to most of them in terms of LOD and linear range, demonstrating promising potential and feasibility for sensitive detection of miRNA. The reasons can be attributed to following factors: (1) The RNA recycling amplification strategy through CHA process was employed to significantly increase the quantity of RNA, making it possible to detect ultra-low concentration of miRNA. In addition to that, the specificity and repeatability of this assay can be improved in the same process. (2) The specially-designed SERS chip, including the uniform 2D AuNPs array, the core-shell metal NPs with embedded SERS reporters and the sandwich nanostructure, is capable of providing abundant “hot-spots” area where localized surface plasmon resonance occurs and leads to local electromagnetic field enhancement at the nanoparticle surface. Consequently, the SERS signals related to target miRNA will be dramatically enhanced. Under the double-enhancement mechanism, the proposed SERS biosensor presents an ultra-sensitive detection feature. Although a few studies reported a lower LOD for miRNA detection, our biosensor has the advantage of better detection reliability owing to the signal calibration process using internal standard molecules, which is essential for potential practical application.

### *3.4. SERS biosensor for the detection of miRNA from clinical human blood samples*

Previous studies have shown that miRNA-21 and miRNA-155 were both oncogenes that were potential biomarkers associated with breast cancer. In light of above excellent properties, we continued to evaluate the feasibility of this SERS biosensor for the detection of miRNAs in clinical human serum samples. As shown in Fig. 4a and b, the expression of miRNA-21 and miRNA-155 from cancer group were both significantly higher than that from normal group based on the data measured by SERS, which is in agreement with the conventional method qRT-PCR (Fig. S4). As shown in Fig. S5, the intensity of the characteristic peaks varied greatly without the CHA system with poor repeatability. After employing the CHA process, the repeatability of SERS spectra was improved significantly, which provided unique opportunity to explore the different features of nucleic acid between cancer and normal group.

Then, we performed principal component analysis and linear discriminant analysis (PCA-LDA) on the SERS results of miRNA-21 and miRNA-155 (Lin et al., 2022). For miRNA-21, when the diagnostic threshold was conventionally set to 0.5, the sensitivity and specificity are 93.3% and 100%, respectively. The both value can be further improved to 100% when the diagnostic threshold was adjusted to 0.88 (Fig. 4b). Similarly, a sensitivity of 100% and specificity of 100% can be

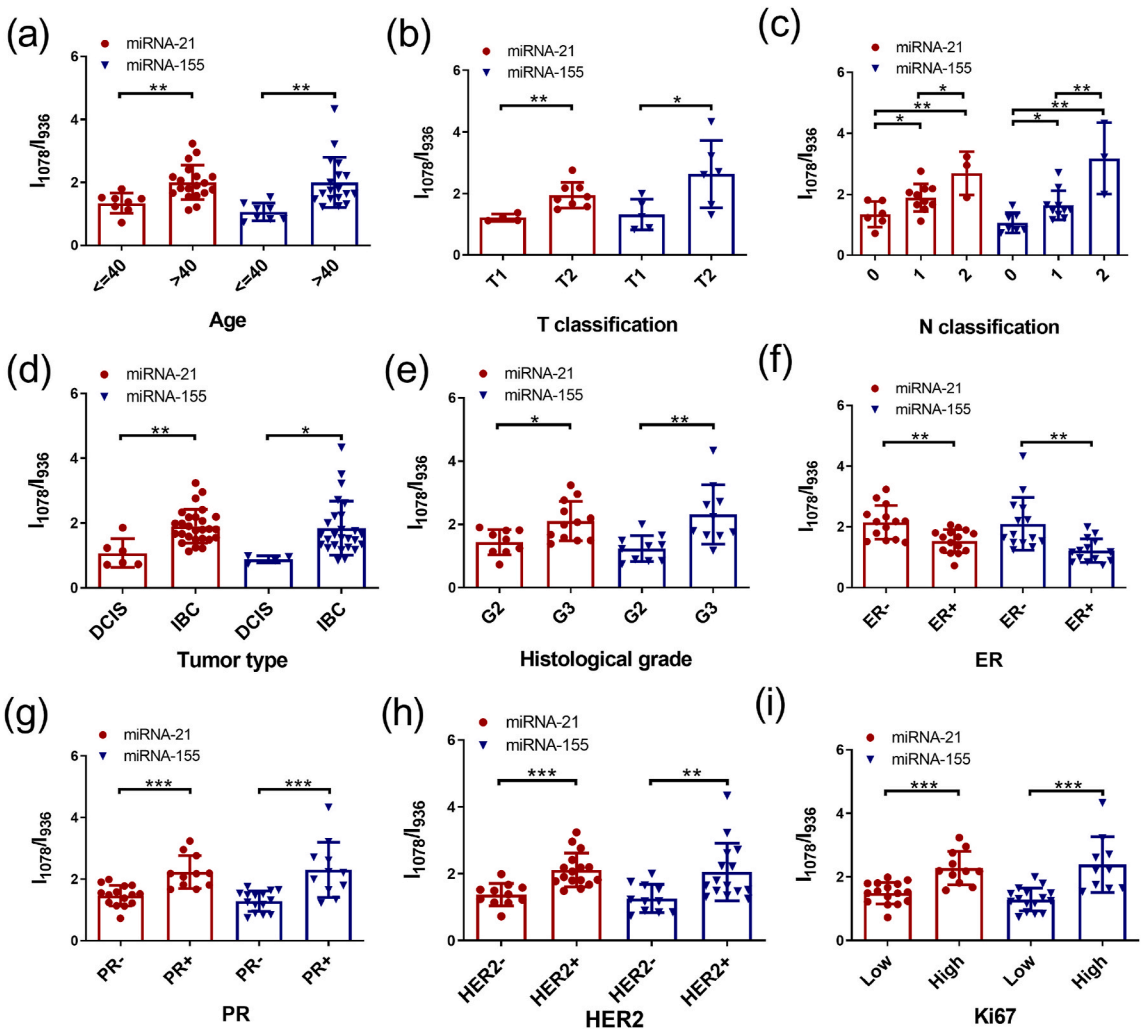


**Fig. 5.** Correlation between the clinical pathological parameters and miRNA-21 and miRNA-155 level detected by the SERS biosensor. Histogram presenting the differential miRNA-21 and miRNA-155 levels in various clinicopathological parameters of breast cancer patients, including (a) Age, (b) T classification, (c) N classification, (d) Tumor type, (e) Histological grade, (f) ER, (g) PR, (h) HER2 and (i) Ki67. DCIS, ductal carcinoma in situ; IBC, invasive breast cancer; +, positive; -, negative; N, lymph node status; T, tumor size. *P value < 0.05. **P value < 0.01. ***P value < 0.001. The sample numbers and exact p-values for each combination are summarized in Table S4.

obtained by adjusting the diagnostic threshold for miRNA-155 data (Fig. 4e). In future clinical application, large-scale sample testing should be conducted to determinate and optimize the cut-off value for miRNA. Besides, the parameters of sensitivity and specificity can be adjusted to meet the requirement of false-positive and false-negative in different clinical scenarios. Further, the operating characteristic curves (ROC) were applied to evaluate the efficiency of cancer detection based on miRNA SERS assay combined with PCA-LDA. The area under curve was calculated to be 1 for both miRNA-21 (Fig. 4c) and miRNA-155 (Fig. 4f) analysis, demonstrating the excellent performance of this method based on miRNA SERS for generating the diagnostic model and identifying cancer subjects from normal ones.

Several reports have shown that miRNA-21 associated significantly with advanced clinical stage, lymph node metastasis and poor prognosis and its expression was found to be up-regulated in both serum and tissues of breast cancer (Savad et al., 2012). Therefore, miRNA-21 could be used as a non-invasive biomarker for breast cancer diagnosis and prognosis as well as an indicator of tumor aggressiveness (Heneghan et al., 2010). For miRNA-155, the overexpression of it leads to apoptosis resistance that triggers an oncogenic cascade response (Chang et al., 2011; Gironella. et al., 2007; Mattiske et al., 2012). It has been reported that miRNA-155 was closely associated with estrogen receptor (ER) and progesterone receptor (PR) status and was found to have increased levels in both serum and tissues of breast cancer patients (Mattiske et al., 2012; Sochor et al., 2014). Accordingly, miRNA-21 and miRNA-155 could be potential promising biomarkers for disease surveillance as oncogenic factors. Thus, we analyzed the correlation between miRNA-21/miRNA-155 and clinic pathological parameters including age, N classification, T classification, tumor type, histological grade, ER, PR, human epidermal growth factor receptor 2 (HER2) and Ki67 in breast cancer patients.

As shown in Fig. 5a, there was a significant elevation in miRNA-21 and miRNA-155 expression levels in patients above age 40 (Han et al., 2017). Among the different stages of N classification and T classification, there were significant differences in the expression of miRNA-21 and miRNA-155 shown in Fig. 5b and c, indicating that the expression levels of miRNA-21 and miRNA-155 might be used to evaluate tumor size and lymphatic metastasis (Chen et al., 2012; Sales et al., 2020; Savad et al., 2012). Ductal carcinoma in situ (DCIS) is known to be a non-obligate precursor of invasive breast cancer (IBC) which is considered to be the most aggressive subtype of breast cancer with consistently poor clinical outcomes and a median overall survival of less than 4 years (Rohan et al., 2021; White et al., 2020). It is noteworthy that miRNA-21 and miRNA-155 were higher expressed in the serum of patients with IBC in

comparison to DCIS (Fig. 5d), suggesting the ability of this biosensor to effectively differentiate between DCIS and IBC and guide the proper treatment. Fig. 5e showed miRNA-21 and miRNA-155 expression levels were significantly increased in G3 stage compared to G2 (Wang et al., 2010; Yadav et al., 2016). The histological grading (HG) of breast cancer is based on the degree of tumor cell differentiation into three HGs: highly differentiated (G1), moderately differentiated (G2) and poorly differentiated (G3), which is one of the most definitive prognostic factors. Of them, G2 is associated with an intermediate risk of recurrence and G3 tumors are the most aggressive (Wang et al., 2016). Hormone levels such as ER, PR and HER2 and Ki67 can be used to determine the molecular type of breast cancer. ER and PR positivity indicates hormone-dependent breast cancer, while Ki67 and HER2 positivity represents a tumor that has high invasiveness and easily recurs and metastasizes to provide a basis for later treatment. Then, we continued to compare the levels of miRNA-21 and miRNA-155 in various groups of breast cancer patients classified by hormonal status (including ER, PR and HER2 and Ki67). Results showed that miRNA-21 and miRNA-155 were highly and significantly expressed in the sera of ER-, PR+, HER2+ and Ki67 high expressing patients (Fig. 5f–i) (Blenkiron et al., 2007; Rodriguez-Martinez et al., 2019; Yadav et al., 2016; Zhu et al., 2009). The above results suggest that miRNA-21 and miRNA-155 can be used to identify molecular types of breast cancer as well as for prognosis prediction. Therefore, development of sensitive and reliable technology such as our proposed SERS-based miRNA biosensor is of imperative clinical value to improve the cancer detection based on miRNA analysis.

## 4. Conclusion

In this study, we have developed a novel biosensor based on SERS integrated with CHA amplification technology for sensitive and reliable detection of miRNA-21 and miRNA-155. The ultra-low detection of limit with 0.398 fM (miRNA-21) and 0.215 fM (miRNA-155) can be achieved due to the double-enhancement mechanism via the RNA recycling amplification strategy and the construction of SERS "hot spots". Besides, the self-calibration process using internal standard molecules enabled a reliable quantitative detection for those miRNA with the $R^2$ of 0.99. Based on these excellent performances, the proposed SERS biosensor is capable of identifying the breast cancer subjects from normal ones with 100% of accuracy, as well as potentially evaluating the molecular types and prognosis for breast cancer. In addition, this method presented the greater dynamic range and lower limit of detection as compared with the conventional qRT-PCR. These results demonstrate that the proposed technology would be an alternative method for the efficient detection of miRNA biomarkers. Notably, this biosensor can be easily modified via different sequences for the detection of other miRNA biomarkers, making it suitable for various cancers diagnosis. Next, more SERS probes will be employed to simultaneously capture multiple miRNAs at one chip with the aim of achieving "multiple-in-one" detection. Finally, minimization of this biosensing platform including portable laser, spectrometer and chip, would be the key step to make it become an ideal point of care (POC) device for liquid biopsy in clinical practice.

## CRediT authorship contribution statement

**Shuyun Weng:** Investigation, Writing – original draft. **Duo Lin:** Methodology, Investigation, Writing – review & editing, Funding acquisition. **Shuxia Lai:** Investigation. **Hong Tao:** Investigation. **Tong Chen:** Validation. **Min Peng:** Methodology. **Sufang Qiu:** Resources. **Shangyuan Feng:** Conceptualization, Supervision, Project administration, Funding acquisition.

## Declaration of competing interest

The authors declare that they have no known competing financial interests or personal relationships that could have appeared to influence the work reported in this paper.

## Acknowledgments

This work was supported by National Natural Science Foundation of China (61975031 and 11974077); The program for Industry University Cooperation Project of Fujian Province (2020Y4006); The Innovation Team Development Plan, Ministry of Education (IRT_15R10); The Special Funds of the Central Government Guiding Local Science and Technology Development (2020L3008). United Fujian Provincial Health and Education Project for Tackling the Key Research (2019-WJ-03).

## Appendix A. Supplementary data

Supplementary data to this article can be found online at https://doi.org/10.1016/j.bios.2022.114236.

## References

Abolghasemi, M., Tehrani, S.S., Yousefi, T., Karimian, A., Mahmoodpoor, A., Ghamari, A., Jadidi-Niaragh, F., Yousefi, M., Kafil, H.S., Bastami, M., Edalati, M., Eyvazi, S., Naghizadeh, M., Targhazeh, N., Yousefi, B., Safa, A., Majidinia, M., Rameshknia, V., 2020. MicroRNAs in breast cancer: roles, functions, and mechanism of actions. J Cell Physiol 235 (6), 5008–5029.

Blenkiron, C., Goldstein, L.D., Thorne, N.P., Spiteri, I., Chin, S.F., Dunning, M.J., Barbosa-Morais, N.L., Teschendorff, A.E., Green, A.R., Ellis, I.O., Tavare, S., Caldas, C., Miska, E.A., 2007. MicroRNA expression profiling of human breast cancer identifies new markers of tumor subtype. Genome Biol 8 (10), R214.

Bruzzone, S., Arrighini, G.P., Guidotti, C., 2003. Electromagnetic response behavior of binary metallic nanoparticles: a comparison of results from a few models of different schematicity. Materials Science and Engineering C 23 (1–2), 191–200.

Chang, S., Wang, R.H., Akagi, K., Kim, K.A., Martin, B.K., Cavallone, L., Kathleen Cuningham Foundation Consortium for Research into Familial Breast, C., Haines, D. C., Basik, M., Mai, P., Poggi, E., Isaacs, C., Looi, L.M., Mun, K.S., Greene, M.H., Byers, S.W., Teo, S.H., Deng, C.X., Sharan, S.K., 2011. Tumor suppressor BRCA1 epigenetically controls oncogenic microRNA-155. Nat Med 17 (10), 1275–1282.

Chang, W., Liu, W., Liu, Y., Zhan, F., Chen, H., Lei, H., Liu, Y., 2019. Colorimetric detection of nucleic acid sequences in plant pathogens based on CRISPR/Cas9 triggered signal amplification. Mikrochim Acta 186 (4), 243.

Chen, J., Wang, B.C., Tang, J.H., 2012. Clinical significance of microRNA-155 expression in human breast cancer. J Surg Oncol 106 (3), 260–266.

Chen, J., Wu, Y., Fu, C., Cao, H., Tan, X., Shi, W., Wu, Z., 2019a. Ratiometric SERS biosensor for sensitive and reproducible detection of microRNA based on mismatched catalytic hairpin assembly. Biosens Bioelectron 143, 111619.

Chen, L., Heikkinen, L., Wang, C., Yang, Y., Sun, H., Wong, G., 2019b. Trends in the development of miRNA bioinformatics tools. Brief Bioinform 20 (5), 1836–1852.

Chen, Y.-X., Zhang, W.-J., Huang, K.-J., Zheng, M., Mao, Y.-C., 2017. An electrochemical microRNA sensing platform based on tungsten diselenide nanosheets and competitive RNA–RNA hybridization. The Analyst 142 (24), 4843–4851.

Chowdhury, P., Ghosh, U., Samanta, K., Jaggi, M., Chauhan, S.C., Yallapu, M.M., 2021. Bioactive nanotherapeutic trends to combat triple negative breast cancer. Bioactive Materials 6 (10), 3269–3287.

Damanti, C.C., Gaffo, E., Lovisa, F., Garbin, A., Di Battista, P., Gallingani, I., Tosato, A., Pillon, M., Carraro, E., Mascarin, M., Elia, C., Biffi, A., Bortoluzzi, S., Mussolin, L., 2021. MiR-26a-5p as a reference to normalize MicroRNA qRT-PCR levels in plasma exosomes of pediatric hematological malignancies. Cells 10 (1), 10.

De la Rosa, C., Reyes, J.L., 2019. Northern blot analysis of microRNAs and other small RNAs in plants. Plant MicroRNAs 121–129.

Dong, H., Lei, J., Ding, L., Wen, Y., Ju, H., Zhang, X., 2013. MicroRNA: function, detection, and bioanalysis. Chem Rev 113 (8), 6207–6233.

Driscoll, A.J., Harpster, M.H., Johnson, P.A., 2013. The development of surface-enhanced Raman scattering as a detection modality for portable in vitro diagnostics: progress and challenges. Phys Chem Chem Phys 15 (47), 20415–20433.

Garcia-Rico, E., Alvarez-Puebla, R.A., Guerrini, L., 2018. Direct surface-enhanced Raman scattering (SERS) spectroscopy of nucleic acids: from fundamental studies to real-life applications. Chem Soc Rev 47 (13), 4909–4923.

Gironella, M., Seux, M.n., Xie, M.-J., Cano, C., Tomasini, R., Gommeaux, J., Garcia, S., Nowak, J., Yeung, M.L., Jeang, K.-T., Chaix, A., Fazli, L., Motoo, Y., Wang, Q., Rocchi, P., Russo, A., Gleave, M., Dagorn, J.-C., Iovanna, J.L., Carrier, A., busque, M.-J.p.P., Dusetti, N.J., 2007. Tumor protein 53-induced nuclear protein 1 expression is repressed by miR-155, and its restoration inhibits pancreatic tumor development. PNAS 104 (41), 16170–16175.

Gong, H., Wu, Y., Zeng, R., Zeng, Y., Liu, X., Tang, D., 2021. CRISPR/Cas12a-mediated liposome-amplified strategy for the photoelectrochemical detection of nucleic acid. Chem Commun (Camb) 57 (71), 8977–8980.

Guk, K., Hwang, S.G., Lim, J., Son, H.-y., Choi, Y., Huh, Y.-M., Kang, T., Jung, J., Lim, E.-K., 2019. Fluorescence amplified sensing platforms enabling miRNA detection by self-circulation of a molecular beacon circuit. Chemical Communications 55 (24), 3457–3460.

Han, J.G., Jiang, Y.D., Zhang, C.H., Yang, Y.M., Pang, D., Song, Y.N., Zhang, G.Q., 2017. A novel panel of serum miR-21/miR-155/miR-365 as a potential diagnostic biomarker for breast cancer. Ann Surg Treat Res 92 (2), 55–66.
Heneghan, H.M., Miller, N., Lowery, A.J., Sweeney, K.J., Newell, J., Kerin, M.J., 2010. Circulating microRNAs as novel minimally invasive biomarkers for breast cancer. Ann Surg 251 (3), 499–505.
Hu, C., Zhang, L., Yang, Z., Song, Z., Zhang, Q., He, Y., 2021. Graphene oxide-based qRT-PCR assay enables the sensitive and specific detection of miRNAs for the screening of ovarian cancer. Anal Chim Acta 1174, 338715.
Iorio, M.V., Ferracin, M., Liu, C.G., Veronese, A., Spizzo, R., Sabbioni, S., Magri, E., Pedriali, M., Fabbri, M., Campiglio, M., Menard, S., Palazzo, J.P., Rosenberg, A., Musiani, P., Volinia, S., Nenci, I., Calin, G.A., Querzoli, P., Negrini, M., Croce, C.M., 2005. MicroRNA gene expression deregulation in human breast cancer. Cancer Res 65 (16), 7065–7070.
Kandettu, A., Radhakrishnan, R., Chakrabarty, S., Sriharikrishnaa, S., Kabekkodu, S.P., 2020. The emerging role of miRNA clusters in breast cancer progression. Biochim Biophys Acta Rev Cancer 1874 (2), 188413.
Kleinman, S.L., Frontiera, R.R., Henry, A.I., Dieringer, J.A., Van Duyne, R.P., 2013. Creating, characterizing, and controlling chemistry with SERS hot spots. Phys Chem Chem Phys 15 (1), 21–36.
Lee, J.U., Kim, W.H., Lee, H.S., Park, K.H., Sim, S.J., 2019. Quantitative and specific detection of exosomal miRNAs for accurate diagnosis of breast cancer using a surface-enhanced Raman scattering sensor based on plasmonic head-flocked gold nanopillars. Small 15 (17), e1804968.
Lin, D., Qiu, S., Chen, Y., Feng, S., Zeng, H., 2022. Multivariate approaches for SERS data analysis in clinical applications. In: Wang, Y. (Ed.), Principles and Clinical Diagnostic Applications of Surface-Enhanced Raman Spectroscopy. Elsevier, pp. 395–431.
Lin, X., Fang, G., Liu, Y., He, Y., Wang, L., Dong, B., 2020. Marangoni effect-driven transfer and compression at three-phase interfaces for highly reproducible nanoparticle monolayers. J Phys Chem Lett 11 (9), 3573–3581.
Ma, D., Huang, C., Zheng, J., Tang, J., Li, J., Yang, J., Yang, R., 2018. Quantitative detection of exosomal microRNA extracted from human blood based on surface-enhanced Raman scattering. Biosens Bioelectron 101, 167–173.
Madzharova, F., Heiner, Z., Kneipp, J., 2020. Surface-enhanced hyper Raman spectra of aromatic thiols on gold and silver nanoparticles. J Phys Chem C Nanomater Interfaces 124 (11), 6233–6241.
Mattiske, S., Suetani, R.J., Neilsen, P.M., Callen, D.F., 2012. The oncogenic role of miR-155 in breast cancer. Cancer Epidemiol Biomarkers Prev 21 (8), 1236–1243.
Mitchell, P.S., Parkin, R.K., Kroh, E.M., Fritz, B.R., Wyman, S.K., Pogosova-Agadjanyan, E.L., Peterson, A., Noteboom, J., O'Briant, K.C., Allen, A., Lin, D.W., Urban, N., Drescher, C.W., Knudsen, B.S., Stirewalt, D.L., Gentleman, R., Vessella, R. L., Nelson, P.S., Martin, D.B., Tewari, M., 2008. Circulating microRNAs as stable blood-based markers for cancer detection. Proc Natl Acad Sci U S A 105 (30), 10513–10518.
Qin, X., Xiao, L., Li, N., Hou, C., Li, W., Li, J., Yan, N., Lin, Y., 2021. Tetrahedral framework nucleic acids-based delivery of microRNA-155 inhibits choroidal neovascularization by regulating the polarization of macrophages. Bioactive Materials 14, 134–144.
Rodriguez-Martinez, A., de Miguel-Perez, D., Ortega, F.G., Garcia-Puche, J.L., Robles-Fernandez, I., Exposito, J., Martorell-Marugan, J., Carmona-Saez, P., Garrido-Navas, M.D.C., Rolfo, C., Ilyine, H., Lorente, J.A., Legueren, M., Serrano, M.J., 2019. Exosomal miRNA profile as complementary tool in the diagnostic and prediction of treatment response in localized breast cancer under neoadjuvant chemotherapy. Breast Cancer Res 21 (1), 21.
Rohan, T.E., Ginsberg, M., Wang, Y., Couch, F.J., Feigelson, H.S., Greenlee, R.T., Honda, S., Stark, A., Chitale, D., Wang, T., Xue, X., Oktay, M.H., Sparano, J.A., Loudig, O., 2021. Molecular markers of risk of subsequent invasive breast cancer in women with ductal carcinoma in situ: protocol for a population-based cohort study. BMJ Open 11 (10), e053397.
Roush, S., Slack, F.J., 2008. The let-7 family of microRNAs. Trends Cell Biol 18 (10), 505–516.
Sales, A.C.V., Gomes da Silva, I.I.F., Leite, M.C.B., Coutinho, L.L., Reis, R., Castoldi, A., Bg Martins, D., Lima-Filho, J.L., Souto, F.O., 2020. Mirna21 expression in the breast cancer tumor tissue is independent of neoadjuvant chemotherapy. Breast Cancer (Dove Med Press) 12, 141–151.
Savad, S., Mehdipour, P., Miryounesi, M., Shirkoohi, R., Fereidooni, F., Mansouri, F., Modarressi, M.H., 2012. Expression analysis of MiR-21, MiR-205, and MiR-342 in breast cancer in Iran. Asian Pac J Cancer Prev 13 (3), 873–877.
Si, Y., Xu, L., Deng, T., Zheng, J., Li, J., 2020. Catalytic hairpin self-assembly-based SERS sensor array for the simultaneous measurement of multiple cancer-associated miRNAs. ACS Sens 5 (12), 4009–4016.
Sochor, M., Basova, P., Pesta, M., Dusilkova, N., Bartos, J., Burda, P., Pospisil, V., Stopka, T., 2014. Oncogenic microRNAs: miR-155, miR-19a, miR-181b, and miR-24 enable monitoring of early breast cancer in serum. BMC Cancer 14, 448.
Song, M., Giovannucci, E., 2016. Preventable incidence and mortality of carcinoma associated with lifestyle factors among white adults in the United States. JAMA Oncol 2 (9), 1154–1161.
Song, S., Lee, J.U., Jeon, M.J., Kim, S., Sim, S.J., 2022. Detection of multiplex exosomal miRNAs for clinically accurate diagnosis of Alzheimer's disease using label-free plasmonic biosensor based on DNA-Assembled advanced plasmonic architecture. Biosensors and Bioelectronics 199, 113864.
Su, J., Wang, D., Norbel, L., Shen, J., Zhao, Z., Dou, Y., Peng, T., Shi, J., Mathur, S., Fan, C., Song, S., 2017. Multicolor gold-silver nano-mushrooms as ready-to-use SERS probes for ultrasensitive and multiplex DNA/miRNA detection. Anal Chem 89 (4), 2531–2538.
Sung, H., Ferlay, J., Siegel, R.L., Laversanne, M., Soerjomataram, I., Jemal, A., Bray, F., 2021. Global cancer statistics 2020: GLOBOCAN estimates of incidence and mortality worldwide for 36 cancers in 185 countries. CA Cancer J Clin 71 (3), 209–249.
van der Hoeven, J.E.S., Deng, T.S., Albrecht, W., Olthof, L.A., van Huis, M.A., de Jongh, P.E., van Blaaderen, A., 2021. Structural control over bimetallic core-shell nanorods for surface-enhanced Raman spectroscopy. ACS Omega 6 (10), 7034–7046.
Wang, F., Zheng, Z., Guo, J., Ding, X., 2010. Correlation and quantitation of microRNA aberrant expression in tissues and sera from patients with breast tumor. Gynecol Oncol 119 (3), 586–593.
Wang, M., Klevebring, D., Lindberg, J., Czene, K., Gronberg, H., Rantalainen, M., 2016. Determining breast cancer histological grade from RNA-sequencing data. Breast Cancer Res 18 (1), 48.
Wang, W., Li, Y., Nie, A., Fan, G.C., Han, H., 2021. A portable SERS reader coupled with catalytic hairpin assembly for sensitive microRNA-21 lateral flow sensing. Analyst 146 (3), 848–854.
White, R.E., Warren, L., Nakhlis, F., Rosenbluth, J., Bellon, J., Block, C., Overmoyer, B., 2020. Characteristics associated with inflammatory breast cancer (IBC): an epidemiologic study from a dedicated IBC program. Breast J 26 (9), 1688–1694.
Williams, Z., Ben-Dov, I.Z., Elias, R., Mihailovic, A., Brown, M., Rosenwaks, Z., Tuschl, T., 2013. Comprehensive profiling of circulating microRNA via small RNA sequencing of cDNA libraries reveals biomarker potential and limitations. Proc Natl Acad Sci U S A 110 (11), 4255–4260.
Wu, J., Zhou, X., Li, P., Lin, X., Wang, J., Hu, Z., Zhang, P., Chen, D., Cai, H., Niessner, R., Haisch, C., Sun, P., Zheng, Y., Jiang, Z., Zhou, H., 2021a. Ultrasensitive and simultaneous SERS detection of multiplex MicroRNA using fractal gold nanotags for early diagnosis and prognosis of hepatocellular carcinoma. Anal Chem 93 (25), 8799–8809.
Wu, Q., Chen, G., Qiu, S., Feng, S., Lin, D., 2021b. A target-triggered and self-calibration aptasensor based on SERS for precise detection of a prostate cancer biomarker in human blood. Nanoscale 13 (16), 7574–7582.
Xu, M., He, Y., Gao, Z., Chen, G., Tang, D., 2014. Isothermal cycling and cascade signal amplification strategy for ultrasensitive colorimetric detection of nucleic acids. Microchimica Acta 182 (1–2), 449–454.
Yadav, P., Mirza, M., Nandi, K., Jain, S.K., Kaza, R.C., Khurana, N., Ray, P.C., Saxena, A., 2016. Serum microRNA-21 expression as a prognostic and therapeutic biomarker for breast cancer patients. Tumour Biol 37 (11), 15275–15282.
Ye, S., Li, X., Wang, M., Tang, B., 2017. Fluorescence and SERS imaging for the simultaneous absolute quantification of multiple miRNAs in living cells. Anal Chem 89 (9), 5124–5130.
Zhang, D., Huang, L., Liu, B., Ni, H., Sun, L., Su, E., Chen, H., Gu, Z., Zhao, X., 2018a. Quantitative and ultrasensitive detection of multiplex cardiac biomarkers in lateral flow assay with core-shell SERS nanotags. Biosens Bioelectron 106, 204–211.
Zhang, K., Lv, S., Lin, Z., Li, M., Tang, D., 2018b. Bio-bar-code-based photoelectrochemical immunoassay for sensitive detection of prostate-specific antigen using rolling circle amplification and enzymatic biocatalytic precipitation. Biosens Bioelectron 101, 159–166.
Zhang, K., Lv, S., Lin, Z., Tang, D., 2017. CdS:Mn quantum dot-functionalized g-C3N4 nanohybrids as signal-generation tags for photoelectrochemical immunoassay of prostate specific antigen coupling DNAzyme concatamer with enzymatic biocatalytic precipitation. Biosens Bioelectron 95, 34–40.
Zhou, Q., Lin, Y., Zhang, K., Li, M., Tang, D., 2018. Reduced graphene oxide/BiFeO3 nanohybrids-based signal-on photoelectrochemical sensing system for prostate-specific antigen detection coupling with magnetic microfluidic device. Biosens Bioelectron 101, 146–152.
Zhu, W., Qin, W., Atasoy, U., Sauter, E.R., 2009. Circulating microRNAs in breast cancer and healthy subjects. BMC Res Notes 2, 89.
Zhu, Y., Wang, Q., Xia, Y., Xiong, X., Weng, S., Ni, H., Ye, Y., Chen, L., Lin, J., Chen, Y., Niu, H., Chen, X., Lin, Y., 2020. Evaluation of MiR-1908-3p as a novel serum biomarker for breast cancer and analysis its oncogenic function and target genes. BMC Cancer 20 (1), 644.
Zhuang, J., Lai, W., Chen, G., Tang, D., 2014. A rolling circle amplification-based DNA machine for miRNA screening coupling catalytic hairpin assembly with DNAzyme formation. Chem Commun (Camb) 50 (22), 2935–2938.
Zia, M.F., Flynt, A.S., 2018. Detection and verification of mammalian mirtrons by northern blotting. miRNA Biogenesis 209–219.